MASTER COPY KEEP THIS COPY FOR REPRODUCTION PURPOSES

REPORT DOCUMENTATION PAGE

Form Approved
OMB No. 0704-0188

1. AGENCY USE ONLY (Leave blank)	2. REPORT DATE	3. REPORT TYPE AND DATES COVERED
	July 17, 1995	FINAL, 9/1/94 - 6/30/95

4. TITLE AND SUBTITLE
Real-Time X-ray Scattering Study of Processing of Thermoplastic Polymers: Effects of Stress

5. FUNDING NUMBERS

6. AUTHOR(S)
Professor Peggy Cebe

7. PERFORMING ORGANIZATION NAME(S) AND ADDRESS(ES)
Massachusetts Institute of Technology
77 Massachusetts Ave.
Cambridge, MA 02139

8. PERFORMING ORGANIZATION REPORT NUMBER

9. SPONSORING/MONITORING AGENCY NAME(S) AND ADDRESS(ES)
U. S. Army Research Office
P. O. Box 12211
Research Triangle Park, NC 27709-2211

10. SPONSORING/MONITORING AGENCY REPORT NUMBER

11. SUPPLEMENTARY NOTES
The view, opinions and/or findings contained in this report are those of the author(s) and should not be construed as an official Department of the Army position, policy, or decision, unless so designated by other documentation.

12a. DISTRIBUTION/AVAILABILITY STATEMENT
Approved for public release; distribution unlimited.

12b. DISTRIBUTION CODE

13. ABSTRACT *(Maximum 200 words)*

Wide and small angle X-ray scattering experiments were conducted on a series of liquid crystalline polycarbonates. These materials are thermotropic and exhibit a monotropic liquid crystalline phase. The mesogen is mono- or di-substituted stilbene, and the flexible spacer is methylene. Fibers were drawn from the mesophase and used in studies of the crystallographic unit cell parameters and thermal transitions. The carbonate linking group between the mesogen and the spacer causes differences in unit cell packing characteristics Although no odd-even effect is found in the thermal transitions, there is a clear odd-even effect seen in the interchain spacings within the unit cells.

14. SUBJECT TERMS	15. NUMBER OF PAGES
Thermoplastic, Liquid Crystalline Polycarbonates, X-ray Scattering, Thermal Analysis	46
	16. PRICE CODE

17. SECURITY CLASSIFICATION OF REPORT	18. SECURITY CLASSIFICATION OF THIS PAGE	19. SECURITY CLASSIFICATION OF ABSTRACT	20. LIMITATION OF ABSTRACT
UNCLASSIFIED	UNCLASSIFIED	UNCLASSIFIED	UL

REAL-TIME X-RAY SCATTERING STUDY OF PROCESSING OF THERMOPLASTICS POLYMERS: EFFECTS OF STRESS

FINAL REPORT
SEPTEMBER 1, 1994 - JUNE 30, 1995

For work performed at:
Department of Materials Science and Engineering
Massachusetts Institute of Technology
Cambridge, MA 02139

Contract Monitor: Dr. Robert Reeber

Professor Peggy Cebe
Department of Physics and Astronomy
Tufts University

July 17, 1995

THE U.S. ARMY RESEARCH OFFICE

CONTRACT No. DAAH04-94-G-0317

TABLE OF CONTENTS

List of Tables

List of Figures

1. HIGHLIGHTS OF DAAH04-94-G-0317 (9/94-6/95)

1.1. Research Accomplishments (experimental method used)

1. Existing miniature motorized tensile stage has been augmented to accommodate a zone heater. First real-time X-ray scattering tension tests were performed at Brookhaven in April 1995. (SAXS)

2. Demonstrated for the first time the use of electron density correlation function to measure long period and crystallinity of liquid crystalline polycarbonates *in-situ* during processing (SAXS) (collaboration with Army Natick)

3. Developed a model of crystallinity development during fiber processing for liquid crystalline polycarbonates (SAXS, WAXS) (collaboration with Army Natick)

4. Completed thermal characterization and X-ray scattering studies of dimethyl-substituted stilbene liquid crystalline polycarbonates (DSC, SAXS, WAXS) (collaboration with Army Natick)

5. Used a novel thermal analysis technique, Modulated Differential Scanning Calorimetry (MDSC) to study formation of the rigid amorphous phase and the existence of multiple endotherms which are created during processing.

1.2 Budget

Amount Spent 9/1/94 - 6/30/95	$ 46,405
Time Period of Expenditure	9 months
Total Budget	$ 97,609
Total Period of Grant	12 months

1.3 Students Supported (months of support) and Present Status

Yao-Yi Cheng (9)	Ph. D., MIT, 2/95; Postdoc. Res. Assoc.
Christine Tsau(5)	S. B., MIT, expected 6/99
Preston Li (4)	S. B., MIT, expected 6/98
Eric Dureiux (4)	S. B., MIT, 6/1995

1.4 Publications and Presentations (Complete citations in 2.1)

Five major publications in refereed journals
Two publications in conference proceedings
Three invited presentations

1.5 Collaborations Established

Dr. Malcolm Capel is beam line manager of the X12B beam at the Brookhaven National Synchrotron Light Source and a faculty member of the *Brookhaven Biology Department*. Dr. Capel is co-author on research performed at NSLS and funded under this contract.

Dr. Heidi Schreuder-Gibson is a synthetic polymer chemist at the *U.S. Army Natick Research, Development and Engineering Center*. We are collaborating on a project in thermotropic liquid crystalline polymers which have application potential in Soldier Protection. I am using real-time x-ray scattering to characterize phase transformations in LCPs synthesized by Dr. Schreuder-Gibson.

Dr. Mary Garbauskas is a scientist at the Corporate Research Center of the *General Electric Corporation*. Dr. Garbauskas became interested in the use of real-time x-ray scattering to study blends made by GE. She is supplying me with blend materials of PBT with polycarbonate.

Dr. Dave Shiraldi is a scientist at *Hoechst Celanese* whom I met at the Asilomar Polymer Physics Conference. Dr. Shiraldi has provided me with a series of polymers of carefully controlled structure in the polyester family.

2. Publications and Presentations Resulting from DAAH04-94-G-0317

2.1 Papers in Refereed Journals

1. Mark V. Brillhart and Peggy Cebe. "Thermal Expansion of the Crystal Lattice in Novel Thermoplastic Polyimides." *J. Polym. Sci., Polym. Phys. Ed.*, 33, 927 (1995).

2. Yao-Yi Cheng, Peggy Cebe, Heidi Schreuder-Gibson, Aaron Bluhm, and Walter Yeomans. "Wide Angle X-ray Scattering Study of Liquid Crystalline Polycarbonates Based on Methyl-Stilbene Mesogen and Methylene-Containing Flexible Spacer." *Molecular Crystals/Liquid Crystals*, in press 1995.

3. Yao-Yi Cheng, Peggy Cebe, Malcolm Capel, Heidi Schreuder-Gibson, Aaron Bluhm, and Walter Yeomans. "Small Angle X-ray Scattering Study of Liquid Crystalline Polycarbonates Based on α-Methyl-Stilbene Mesogen and Methylene-Containing Flexible Spacer." *J. Polym. Sci., Polym. Phys. Ed.*, accepted 7/95.

4. Yao-Yi Cheng, Peggy Cebe, Malcolm Capel, Heidi Schreuder-Gibson, Aaron Bluhm, John Stapler, and Walter Yeomans. "X-ray Scattering and Thermal Characterization of α,β-Dimethyl Stilbene Polycarbonates." *Molecular Crystals/Liquid Crystals*, in review 5/95.

5. Yao-Yi Cheng, Mark Brillhart, Peggy Cebe, and Malcolm Capel. "Small Angle X-ray Scattering, Thermal and Mechanical Analysis of Poly(butylene terephthalate)/Polycarbonate Blends." *Macromolecules*, in preparation for submission 7/95.

2.2 Papers in Conference Proceedings

1. Mark V. Brillhart, Peggy Cebe, and Malcolm Capel. "Real-Time X-ray Scattering of Binary Polymer Blends: Poly(butylene terephthalate)/ Polycarbonate," Denver X-ray Conference, in press 1995.

2. Yao-Yi Cheng, Peggy Cebe, Malcolm Capel, Heidi Schreuder-Gibson, Aaron Bluhm, and Walter Yeomans. "Crystallization of Monotropic Liquid Crystalline Polycarbonates Based on α-Methyl Stilbene Mesogen," 24th NATAS Conference Proceedings, in press 1995.

2.3 Invited Talks

July 1995, "Real-Time Small-Angle X-ray Scattering from Blends," American Crystallographic Assoc. Conference, Montreal, CN.

September 1995, "Crystallization of Monotropic Liquid Crystalline Polycarbonates Based on α-Methyl Stilbene Mesogen,"," North American Thermal Analysis Soc. Conference, San Francisco, CA.

December 1995, "Real-Time Small-Angle X-ray Scattering from Blends." 1995 International Chemical Congress of Pacific Basin Societies, Honolulu, HA.

3.0 RESEARCH ACCOMPLISHMENTS

The purposes of the research were to use real-time X-ray scattering: 1.) to assist in development of a model for the effects of stress imparted during processing, and 2.) to study the kinetics of crystal structure development in stressed and unstressed thermoplastic polymers. Three parallel lines of research were conducted. The first tasks involved real-time X-ray scattering experiments to complete our collaborative study with the researchers at the U.S. Army Natick Labs. The second tasks involved static X-ray and thermal characterization studies of the materials. The third tasks involved the practice run at which we used our tensile stage for the first time to acquire real-time data under conditions of applied stress.

Since beam time at the Brookhaven National Synchrotron Light Source (NSLS) is given in discrete blocks, our real-time X-ray studies were performed over a total of three trips. Data from the first two trips is analyzed and has been published or will appear in 1995. Data from the last trip (April 1995) have not been analyzed because at MIT we did not have access to a Fortran compiler for our Silicon Graphics Workstation. Two dimensional data could not be viewed and analyzed. This will be one of the first tasks of a new student, since we now have, at Tufts, access to the Fortran compiler of the High Energy Physics group.

Our collaboration with Dr. Malcolm Capel has proven to be extremely beneficial, and we have been very successful in getting beam time allocated through the NSLS General Users Program. Our last proposal, for beam time in 1994-1996, was rated very highly at 1.9 (1.0 is highest, 5.0 lowest) and we received 18 days of beam time. In the following sections we summarize our studies involving collaborative work with the U. S. Army Natick group on liquid crystalline polycarbonates.

3.1 Materials and Experimental Techniques

3.1.1 Materials

Main chain thermotropic liquid crystalline polymers (LCPs) consisting of a rigid mesogen alternating with a flexible spacer have been studied extensively. Stilbene-containing polymers have been widely studied because of the straightforward synthesis of the stilbene, which was evaluated as a synthetic bovine hormone [2]. α–methyl substituted stilbene (HMS) has been used as a mesogenic unit to form LCPs containing methylene units as the flexible spacer. The linking group between the mesogen and the flexible spacer may be an ether [3], an ester [4,5], or, in our research program, a carbonate [6]. The structural formula for our liquid crystalline polycarbonates is:

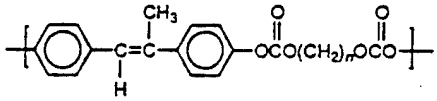

The flexible spacer number, n, ranges from n = 4-10,12. We will refer to these polycarbonate based LCPs as HMS-n. When both hydrogens on the stilbene mesogen are replaced by methyl, we refer to these di-methyl substituted polymers as DMS-n.

The synthesis of HMS polycarbonates and has been published separately [1]. The resultant LCPs were soluble in chloroform and obtained as fine white powders, except for n=7,9 which were obtained as white, very fibrous product. All polymers studied in this research have reasonably high weight average molecular weight, in the range from 11,000 to 54,800 with distributions (M_W/M_n) close to 2 [1].

3.1.2 Wide Angle X-ray Scattering (WAXS)

WAXS studies were made in reflection mode for all unoriented HMS polycarbonates. A Rigaku RU-300 rotating anode X-ray generator was used to examine samples in $\theta/2\theta$ reflection mode. The diffractometer has a diffracted beam graphite monochromator. Copper K_α radiation (λ = 1.54Å) was used with a step scan interval of 0.1 degree, at a scan rate of 1 degree/minute over the 2θ range from 3 to 53 degrees. HMS powder was melted on a teflon substrate then cooled, and the resulting solid piece was fixed to an aluminum frame for examination by WAXS. To form thin film samples, some powders were also dissolved in chloroform and several drops of the solution were placed onto quartz substrates. The thin films were run "as-is" without any other thermal treatment.

3.1.3 Wide Angle X-ray Scattering Fiber Pattern

WAXS in transmission mode was performed at room temperature on selected oriented HMS fibers, using a Philips PW1830 X-ray generator operated at 45kV and 45mA with Ni-filtered CuK_a radiation. The Statton camera used in this study consists of a pinhole collimator over which the sample is placed, and a flat film (Kodak DEF-5) to record the scattering pattern. The sample to film distance is calibrated using Si powder reference standard (from National Institute of Standards & Technology) rubbed on the sample surface. The first 2θ value for Si is 28.44°. HMS fibers were hand drawn from the mesophase using tweezers. It was relatively easy to draw fibers for HMS-5,7, and 8 but quite difficult to draw HMS-6. The hand drawn fibers cooled rapidly in air, and will be referred to as raw fiber. Raw fibers were subsequently annealed below the melting temperature. WAXS was performed on both the raw and annealed fibers.

3.1.4 Differential Scanning Calorimetry (DSC)

Thermal properties of materials were studied using a Perkin-Elmer DSC-4 or DSC-7. Indium was used to calibrate the temperature and the heat of fusion. The studies that were done included heating and cooling at fixed rates, and isothermal crystallization to test the effect of crystallization temperature on both crystallization time and melting temperature.

The first approach involved heating and cooling at fixed rates over a wide temperature interval. The sample was heated to 200°C and held at that temperature for 2.5-3 minutes, then cooled at a rate of 10°C/min to 40°C, then heated at 10°C/min to 200°C. This study was done for all DMS-n samples. For the purpose of comparison, HMS-7 was also studied in the same way. In addition, HMS-7 and DMS-7 were cooled and heated at 5, 20, and 50°C/min. HMS-7 was also cooled at 2°C/min. This study was designed to test the dependence of the isotropic to mesophase transition temperature on cooling rate.

The next study was isothermal crystallization for HMS-7 and DMS-7. The sample was melted at 200°C for about 3 minutes, then quenched at -50°C/min to a crystallization temperature T_C and held isothermally until the crystallization was finished. The T_Cs were specifically chosen in advance to keep the crystallization times comparable. Because DMS-7 has lower crystallization temperature than HMS-7, we chose a crystallization temperature in the range from 120 to 132°C for DMS-7 and from 136°C to 147°C for HMS-7. Exothermic heat flow as a function of time was large enough to be measured at the chosen temperature for both materials. Here we were interested in the isothermal crystallization kinetics.

The next study involved immediate rescan after isothermal crystallization for HMS-7 and DMS-7. After staying at T_C isothermally until crystallization was finished, the sample was immediately heated at 5°C/min to 190°C without cooling. This immediate rescan technique avoids the formation of imperfect crystals during cooling to room temperature, and thus results in a cleaner endothermic response.

3.1.5 Small Angle X-ray Scattering (SAXS)

The X12B beam line at Brookhaven National Synchrotron Light Source (NSLS) was used to obtain small angle X-ray scattering data in transmission mode. For high temperature work, a Mettler hot stage was supported in the X-ray beam path by an aluminum holder, and the beam passed through the sample, which was sealed between two pieces of Kapton™ tape. A gas-filled two-dimensional histogramming wire detector was used. For isotropic samples, circular integration of the intensity was used to enhance the signal to noise ratio. For oriented fiber samples, sectorial integration of the intensity was used with 10° interval in each section. The beam profile was treated according to pinhole geometry. SAXS data were taken on two separate trips. The sample to detector distance was 1.39 m or 1.85 m, and was calibrated by cholesterol meristate and collagen fiber. X-ray wavelength was 1.38Å or 1.53Å.

SAXS scans at room temperature were taken for DMS-5 to 8, which were non-isothermally crystallized by cooling at 5°C/min from the melt to room temperature. Real-time SAXS data were taken for an isothermal crystallization study. DMS-7 and 8 samples were melted at 190°C for 2.5-3 minutes, then cooled at 20°C/min to 124°C

and held there until crystallization was finished. Data were collected during cooling from 170 to 140°C and during the whole isothermal crystallization process. The data collection time was 10 seconds. Raw HMS-7 fiber was quickly heated from room temperature to 88°C, then heated at 20°C/min to 138°C. Similarly, raw DMS-7 fiber was quickly heated to 75°C, then heated at 20°C/min to 125°C. Data were collected during the 20°C/min heating process. The data collection time was 15 seconds.

Lorentz corrected SAXS intensity, Is^2, (where s is the scattering vector, $s = 2 \sin\theta/\lambda$) was also corrected for background, sample absorption, variation of incident beam intensity and thermal density fluctuations. The slope of Is^4 versus s^4 plot was used to get the diffraction intensity contribution from thermal density fluctuations. The corrected intensity is used for quantitative analysis.

3 .2 Wide Angle X-ray Scattering Studies of Fibers

X-ray diffraction patterns of raw fibers drawn from the mesophase revealed that the stability of the mesophase decreases as the methylene spacer length gets close to that of mesogen. From X-ray diffraction patterns of annealed fibers and molecular modeling studies, the unit cell parameters of HMS-5 to 8 were determined. HMS-5 and 6 have an orthorhombic structure while HMS-7 and 8 have a monoclinic structure. More important, an odd-even oscillation is observed in the d-spacings of the (020) and (110) reflections as a function of n, which relates to differences in interchain packing in the odd and even members of the series. All HMS-5 to 8 have a stable intermeshed crystal structure in which the mesogen and the flexible spacer group on adjacent chains are aligned. In this structure, the disposition of the carbonate group differs from n-even to n-odd, and is responsible for the odd-even effect seen in the two dominant interchain d-spacings. We suggest the higher degree of overlap of the carbonate linkage of HMS-7 and 8 might be the reason for their less stable mesophase compared with HMS-5 and 6.

Although both α–methyl stilbene polyethers [3] and α–methyl stilbene polyesters [4,5] are enantiotropic LCPs, our recent study of α–methyl stilbene polycarbonates showed that these LCPs only have a monotropic liquid crystalline phase [6]. Similar monotropic liquid crystalline behavior of other main chain thermotropic LCPs has been observed [7-15]. The distinction is made based on whether or not the mesophase (lc) is stable and can be observed separately from the crystalline phase (k) during cooling from the isotropic (i) melt or during heating [16]. In enantiotropic LCPs, the mesophase is stable with respect to the crystalline phase, and both thermal transitions can be observed in heating and cooling. In other words, $T_{i\text{-}lc}$ and $T_{lc\text{-}k}$ (in cooling) and $T_{k\text{-}lc}$ and $T_{lc\text{-}i}$ (in heating) can be separately identified. In monotropic LCPs, the mesophase is not stable with respect to the crystalline phase. During heating, the $T_{lc\text{-}i}$ transition is always masked by the crystalline melting transition; and, during cooling, the $T_{i\text{-}lc}$ transition can be

observed only provided that crystallization is suppressed. In our previous research, we have shown that changing the linking group to carbonate is sufficient to alter the stability of the mesophase, resulting in a monotropic liquid crystalline phase [6].

In addition to the difference in stability range of the mesophase, there are also differences in the observed odd-even effect between the HMS-polyethers/polyesters and our polycarbonates. The odd-even effect refers to the oscillation of certain parameters as a function of whether the flexible spacer number n is odd or even. An odd-even effect is usually seen for main chain thermotropic LCPs [17-22] in such properties as 1.) the transition temperatures $T_{k\text{-}lc}$, $T_{lc\text{-}i}$; 2.) the heats of transition, $\Delta H_{lc\text{-}i}$; and 3.) the entropy factor, $DS_{lc\text{-}i}$. This phenomenon has been observed for α–methyl stilbene polyethers [3] and α–methyl stilbene polyesters [4,5]. In our HMS polycarbonates, the monotropic nature of the mesophase prevents observation of some of the thermal transitions [6]. Therefore, the odd-even effect in the thermal properties is not obvious because of their monotropic liquid crystalline behavior [6]. However, we did observe that all transition temperatures dropped when n exceeded eight [6]. In addition, in our HMS polycarbonates an interesting odd-even effect has been observed (and reported in preliminary form [23]) in the two dominant interchain d-spacings from the wide angle X-ray scattering powder diffraction pattern when n ranges from 5 to 8. When n exceeded eight, the major interchain d-spacings leveled off.

HMS polyethers, polyesters, and polycarbonates all contain the same stilbene mesogen and the same flexible spacer group. These LCPs differ only in their linking groups. The question arises concerning the aspects of chain structure that cause our HMS polycarbonates to be monotropic LCPs, and to show weak (or no) odd-even effect in their thermal transitions, compared to their chemical relatives. We suggested previously that the stability of the liquid crystalline phase is affected by the carbonate linkage, which causes fast crystallization resulting from intermolecular interaction [6].

The WAXS diffractometer scans of HMS-5-12 are shown in Figure 1. WAXS scans in reflection mode generally show two sharp and dominant interchain reflections. In addition, several HMS polycarbonates show a number of much weaker peaks. Considering only the two dominant interchain reflections, we show in Figure 2a a plot of d-spacing vs. flexible spacer number, n. An odd-even effect is observed in both the higher and lower d-spacings for $n = 5$ to 8. When $n \geq 9$, the two major d-spacings get closer to one another and level off. In Figure 2b, the d-spacings are shown for n=5 to 8, designated according to their Miller index assignment.

Next, we show the flat film fiber patterns of raw (unannealed) fibers, and annealed fibers. In Figure 3 WAXS of selected raw fibers is shown. HMS-5 raw fiber is shown in Figure 3a and HMS-8 is shown in Figure 3b. HMS-5 raw fiber WAXS shows a single diffuse equatorial maximum and no meridional reflections, which is characteristic of a nematic mesophase. HMS-8 raw fibers have two diffuse equatorial

reflections and no meridional reflections. The appearance of two diffuse equatorial maxima in HMS-8 indicates a better interchain registry between the polymer chains in these fibers. For the sake of brevity, HMS-6 and HMS-7 are not shown. HMS-6 raw fiber was similar to HMS-5, and HMS-7 was similar to HMS-8.

WAXS patterns of selected annealed HMS fibers are shown in Figure 4. Once the raw fiber is annealed, crystalline reflections are observed though some are too weak to be seen in the reproduction. In Figure 4a, HMS-5 annealed fiber WAXS is shown along with a sketch of the reflections in Figure 4b. One meridional reflection is seen in annealed HMS-5 along with two equatorial and five quadrantal reflections. In Figure 4c, annealed fiber WAXS of HMS-8 is shown, with a sketch in Figure 4d. Two equatorial and six quadrantal reflections are identified in HMS-8. There were no meridional reflections in HMS-8. HMS-6 and HMS-7 patterns are not shown. HMS-6 did not form highly oriented fibers upon annealing, though numerous crystalline reflections were seen as broad arcs. HMS-7 annealed fiber pattern is similar to that of HMS-8. Experimental 2θ angles and corresponding d-spacings for HMS-5-8 are listed in Tables 1-4, respectively, for the annealed fibers.

In the raw fibers shown in Figure 3, there is an absence of three dimensional crystalline order. Two raw fibers, HMS-5 and 6, showed a single equatorial reflection, an indication that the nematic mesophase could be described by a single average interchain separation distance. The other two raw fibers, HMS-7 and 8, displayed two strong equatorial reflections, an indication that for these fibers the nematic mesophase would best be described by two different average interchain separation distances. These probably reflect a higher level of order in the packing for HMS-7 and 8. When the three dimensional crystals form out of the nematic phase, which serves as the template on which crystals will nucleate, the average interchain spacing of the crystals is represented by the two strong equatorial reflections which are associated with the (020) and (110) planes.

The interchain spacing of the nematic mesophase seen in the raw fiber WAXS (Figure 3) can be compared to the interchain spacings of the crystalline phase seen in the annealed fiber WAXS (Figure 4). For HMS-5 (Figure 3a) and HMS-6 (not shown) the single equatorial reflection seen in the pattern of the raw, unannealed fiber has a d-spacing which lies in between the d-spacings of the two strongest reflections seen in the annealed fiber powder pattern. The inner spot on the equator of HMS-8 raw fiber pattern (Figure 3b), lies on the (020) position of annealed fiber pattern (Figure 4b). The outer diffuse spot has a d-spacing which lies in between the d-spacings of the two strongest reflections seen in the powder pattern just as the single equatorial reflection does in the HMS-5 and 6 raw fiber pattern. In contrast, the two spots on the each side of equator in the HMS-7 raw fiber pattern have d-spacings close to the d-spacings of the two strongest reflections seen in the powder pattern. For annealed fibers HMS-8 (Figure 4b) and HMS-7 (not shown) the d-spacings of the two strongest equatorial reflections correspond to the two strongest reflections observed in the powder patterns of Figure 1.

3.3 X-ray Scattering and Thermal Characterization of DMS

In this work, we focus on the characterization of a,ß-dimethyl stilbene (DMS) polycarbonates and on the comparison between them and α–methyl stilbene (HMS) polycarbonates. The wide angle X-ray scattering pattern shows that DMS polycarbonates are able to form a liquid crystalline phase. However, their liquid crystalline phase is generally not stable with respect to the crystalline phase. From differential scanning calorimetry cooling scans at various cooling rates, the liquid crystalline phase transition of DMS polycarbonates can not be separated from their crystalline phase transition, unlike that of HMS polycarbonates, which can. This is because the steric effect of the second lateral methyl substituent on the stilbene mesogen lowers the stability of the liquid crystalline phase of DMS polycarbonates. Small angle X-ray scattering studies were performed on the DMS polycarbonates to examine the structure of the crystalline phase. In general, DMS polycarbonates have higher values of linear crystallinity and crystal thickness than HMS polycarbonates. Also, DMS polycarbonates do not have "odd-even" property oscillation with the methylene spacer length, unlike HMS polycarbonates which do. We suggest that this may be caused by the possible loss of carbonate dipole interaction caused by the steric effect of the second methyl substituent.

The polycarbonates with heptane flexible spacer (n=7) were chosen for comparison of the effect of different mesogen substitution on their properties [1]. Polycarbonates with either mono- or di-methyl substituted stilbene mesogen (HMS-7 and DMS-7) are semicrystalline and appear to be liquid crystalline under the optical microscope [1].

It is believed that the insertion of substituents on the mesogen will lower the stability of the liquid crystalline phase because of the steric effect [24-32]. For example, a,ß-dimethyl stilbene polyesters do not have an enantiotropic liquid crystalline phase while α–methyl stilbene polyesters do [3,24,31]. In this work, we show that DMS polycarbonates do only have a virtual liquid crystalline phase. The effect of the insertion of the second methyl substituent on the stilbene mesogen on the crystallization behavior and crystalline structure is also investigated.

Figure 5 shows WAXS reflection pattern of DMS-7 film. The narrow single peak maximum located at d-spacing 4.4Å suggests the existence of the nematic liquid crystalline order. Nematic order was also observed using polarizing optical microscopy [1].

In the DSC cooling scan of DMS-4-10 and 12 cooling from the melt, usually a broad exotherm with a low temperature tail is observed, as shown in Figure 6a. In the reheating scan shown in Figure 6b, a broad endotherm with a low temperature tail caused by the melting of less perfect crystals is usually observed for most DMS samples. Table 5 summarizes the melting and crystallization peak positions for DMS-4-10 and 12. The extremely low crystallization temperature for DMS-5 was

reproducible. The transition temperatures of DMS polycarbonates do not have an obvious relationship with the flexible spacer number, unlike HMS polycarbonates, which have close transition temperatures when the flexible spacer number ranges from n=5-8 [6]. Nevertheless, for both HMS and DMS polycarbonates, the transition temperatures drop when methylene spacer number, n, is bigger than 8.

For the purpose of comparison, Figure 7a,b shows the cooling and reheating scans of DMS-7 and HMS-7. In both scans, the baseline of HMS-7 is tilted steeply down from left to right. DMS-7 has lower crystallization and melting temperature than HMS-7. In cooling, Fig. 7a, DMS-7 shows a single broad exotherm. HMS-7 shows a double exotherm with a small, sharp isotropic to nematic ($T_{i\text{-}lc}$) transition followed by a much larger, sharp crystallization ($T_{lc\text{-}k}$) transition.

Figure 8a,b shows DSC cooling scans at various cooling rates for DMS-7 and HMS-7, respectively. DMS-7 has a single broad exotherm for all rates. HMS-7 has a large sharp exotherm followed by a broad low temperature tail at all rates. In addition, for rates of 10°C/min or higher, the isotropic to nematic ($T_{i\text{-}lc}$) transition is seen clearly on the high temperature side of the main exotherm. As described previously [6], HMS-7 has a monotropic liquid crystalline phase, which can be observed in cooling only provided that the crystallization process is suppressed, for example, by increasing the cooling rate. The small higher temperature exotherm seen in Figure 8b represents the isotropic to liquid crystalline phase transition, $T_{i\text{-}lc}$, whose position is less affected by the cooling rate, compared with that of the large lower temperature crystallization exotherm. Therefore, at a slow cooling rate like 2°C/min, the isotropic to liquid crystalline phase transition is covered by the crystalline phase transition. But at higher cooling rates, the liquid crystalline transition can be observed for HMS-7. In contrast, for DMS-7 shown in Figure 8a, higher cooling rates up to 50°C/min still can not separate the liquid crystalline transition from the crystalline phase transition.

We show in Figure 9a,b the Lorentz corrected SAXS intensity (Is^2) versus s data at room temperature of DMS-7 and HMS-7, respectively, which had been cooled at 5°C/min from the melt to room temperature. Considering that spherulites have been observed by optical microscopy [1], we assume that DMS polycarbonates have a lamellar structure in which stacks of lamellae alternate with amorphous material. Then the one-dimensional electron density correlation function, K(z), is obtained by discrete Fourier transform of the Lorentz corrected intensity. z is a dimension along the normal to the lamellar stacks which have a stack periodicity, L, also called the long period. Long period, crystal thickness, l_c, and linear crystallinity within the stacks, χ_c, are obtained according to the method of Strobl and Schneider [33].

In Table 6, we list long period, linear crystallinity, and crystal thickness at room temperature for DMS-5 to 8 and HMS-5 to 8 crystallized by cooling at 5°C/min from the melt to room temperature. DMS-6, 7 and 8 have similar values of linear crystallinity. But DMS-7 has higher value of crystal thickness and long period.

With the exception of HMS-5, the HMS polycarbonates have higher values of long period, and lower values of linear crystallinity and crystal thickness than DMS polycarbonates with the same n number. HMS-5 reverses these trends compared to DMS-5. This is probably a result of the slower crystallization kinetics in DMS-5 which causes lower crystallization temperature and less perfect crystal structure, as shown in Figure 5 and Table 5.

In Figure 10, we show Lorentz corrected intensity (Is^2) versus s data for the real-time SAXS study of isothermal crystallization of DMS-7. The sample was melted and then cooled to 124°C. The first scan at the bottom, marked T = 154°C, is from the melt. The second scan from the bottom, marked t = 0, represents the initial stage of isothermal crystallization at 124°C. Notice that by the time the cooling process from 154°C to 124°C is completed, significant intensity has already developed. Electron-dense phase formation does happen during the cooling process as DMS-7 is cooled through the isotropic to liquid crystalline transition.

The annealed HMS-7 and DMS-7 fibers display nice oriented fiber SAXS patterns (data not shown). The intensity maxima are located on the meridian and elongate in the direction of the equator, which is due to misorientation of the crystallites. The intensity of the meridian section is used to obtain linear crystallinity, crystal thickness and long period from the one-dimensional electron density correlation function for annealed DMS-7 and HMS-7 fibers, as listed in Table 7. Annealed DMS-7 and HMS-7 fibers have similar values of crystal thickness, but DMS-7 has higher linear crystallinity and lower long period.

3.4. Discussion

The cross-section of the stilbene unit of DMS polycarbonates is 8.6 Å, which is much larger than that of HMS polycarbonates, at 6.5 Å [1]. Therefore, we expect some differences in behavior between the two groups of polycarbonates due to steric packing differences. First of all, we notice that unlike HMS polycarbonates, DMS polycarbonates have only one broad exotherm. Also, the liquid crystalline phase transition can not be separated from the crystalline phase transition during cooling even at higher cooling rates. These facts suggest that DMS polycarbonates have less stable liquid crystalline phases than HMS polycarbonates do. The second lateral substituent on the mesogen further reduces the thermal stability of the liquid crystalline phase. This phenomenon has been observed in other LCPs [3,24,31]. The second lateral substituent on the mesogen separates the polymer chains further, which reflects in the larger crystal unit cell dimension for DMS-7 compared with HMS-7. The unit cell parameters relating to interchain distances are b and $a\sin\beta$ (where b = 90° for DMS-7). The area of the basal plane, the product of b and $a\sin\beta$ parameters, is 41.9 $Å^2$ for HMS-7, which is smaller than 43.6 $Å^2$ for DMS-7.

The closeness of adjacent polymer chains of HMS-7 compared to those of DMS-7 is also reflected in the raw fiber WAXS pattern. DMS-7 raw fiber pattern only shows a single diffuse maximum on the equator, which is characteristic of a nematic mesophase. However, HMS-7 raw fiber pattern displays two equatorial reflections, which reflects a higher level of order in the interchain packing.

Because of the steric effect of the second lateral substituent on the mesogen, DMS polycarbonates do not seem to have "odd-even" property oscillation with the methylene spacer length, unlike HMS polycarbonates which do show such oscillation. DMS-7 does not exist in a stable intermeshed structure like HMS-7 does. It is our supposition that the steric effect of the second methyl substitution on the mesogen reduces the carbonate dipole interaction between adjacent polymer chains. Therefore, the transition temperatures do not change regularly with the methylene spacer length for DMS polycarbonates. DMS-7 and 8 seem to have close crystallization and melting transition temperatures. When DMS-7 and 8 are isothermally crystallized at 124°C, they have similar values of linear crystallinity, crystal thickness, and long period. Though the crystal thickness and long period are higher for DMS-7 than DMS-8 when both are cooled at 5°C/min from the melt, it is probably because a large population of less perfect crystalline lamellae are formed during the cooling process for DMS-8.

3.5. Conclusions

HMS polycarbonates with 5 to 8 methylene flexible spacer units have a stable intermeshed crystal structure. Within this structure, the disposition of the carbonate group differs from n-even to n-odd and causes the odd-even effect of the crystal unit cell parameters, b and asinb. Furthermore, the higher degree of overlap of the carbonate linkage of HMS-7 and 8 than HMS-5 and 6 between adjacent polymer chains may be the reason why HMS-7 and 8 have less stable mesophase than HMS-5 and 6.

The steric effect of the second lateral methyl substituent on the stilbene mesogen lowers the stability of the liquid crystalline phase of DMS polycarbonates. Therefore, DMS polycarbonates only have a virtual liquid crystalline phase, unlike HMS polycarbonates which are able to form a monotropic liquid crystalline phase. Although both HMS and DMS polycarbonates are fast crystallizing materials, DMS polycarbonate crystallizes at lower temperature than HMS polycarbonate for comparable spacer length. DMS polycarbonates do not have "odd-even" property oscillation with the methylene spacer length, unlike HMS polycarbonates which do [3,4]. We suggest that this may be caused by the possible loss of carbonate dipole interaction caused by the steric effect.

4. REFERENCES

1. A. L. Bluhm, P. Cebe, H. L. Schreuder-Gibson, J. T. Stapler and W. Yeomans, *Mol. Cryst. Liq. Cryst.* **239**, 123 (1994).
2. E. C. Dobbs, L. Goldberg, W. Lawson and R. Robinson, *Proc. Roy. Soc.* **B127**, 140 (1939).
3. V. Percec, T. D. Shaffer and H. Nava, *J. Polym. Sci., Polym. Lett.* **22**, 637 (1984).
4. A. Ruviello and A. Sirigu, *Makromol. Chem.* **183**, 895 (1982).
5. A. Blumstein, *Polym. J.* **17(1)**, 277 (1985).
6. Y.-Y. Cheng, P. Cebe, H. Schreuder-Gibson, A. Bluhm and W. Yeomans, *Macromolecules* **27**, 5440 (1994).
7. R. Pardey, A. Zhang, P. A. Gabori, F. W. Harris, S. Z. D. Cheng, J. Adduci, J. V. Facinelli and R. W. Lenz, *Macromolecules* **25**, 5060 (1992).
8. F. Papadimitrakopoulos, S. L. Hsu and W. J. MacKnight, *Macromolecules* **25**, 4761 (1992).
9. F. Papadimitrakopoulos, E. Sawa and W. J. MacKnight, *Macromolecules* **25**, 4682 (1992).
10. V. Percec and Y. Tsuda, *Macromolecules* **23**, 3509 (1990).
11. V. Percec and R. Yourd, *Macromolecules* **22**, 524 (1989).
12. V. Percec and R. Yourd, *Macromolecules* **22**, 3229 (1989).
13. S. Z. D. Cheng, M. A. Yandrasits and V. Percec, *Polymer* **32**, 1284 (1991).
14. M. Yandrasits, S. Z. D. Cheng, A. Zhang, J. Cheng, B. Wunderlich and V. Percec, *Macromolecules* **25**, 2112 (1992).
15. K. Fujishiro and R. W. Lenz, *Macromolecules* **25**, 81 (1992).
16. V. Percec and A. Keller, *Macromolecules* **23**, 4347 (1990).
17. R. B. Blumstein and A. Blumstein, *Mol. Cryst. Liq. Cryst.* **165**, 361 (1988).

18. A. Blumstein and O. Thomas, *Macromolecules* **15**, 1264 (1982).

19. A. Blumstein, *Polym. J.* **17(1)**, 277 (1985).

20. A. M. Donald and A. H. Windle, *Liquid Crystalline Polymers* (Cambridge University Press, Cambridge, 1992), Chap. 3.

21. A. Abe, *Macromolecules* **17**, 2280 (1984).

22. D. Y. Yoon and S. Bruckner, *Macromolecules* **18**, 651 (1985).

23. P. Cebe, J. Carbeck and H. Schreuder-Gibson, *Polym. Preprints* **33(1)**, 331 (1992).

24. A. Sirigu, In *Liquid Crystallinity in Polymers: Principles and Fundamental Properties*, ed. by A. Ciferri, VCH Publishers, New York, 1991, Chapter 7.

25. J. Asrar, O. Thomas, Q. Zhou and A. Blumstein, *Proc. Macro-IUPAC*, Amherst, 1982.

26. A. Blumstein, S. Vilasagar, S. Ponrathnam., S.B. Clough, R.B. Blumstein and G. Maret, *J. Polym, Sci., Polym. Phys. Ed.* **20**, 877 (1982).

27. B.W. Jo, R.W. Lenz and J.I. Jin, *Makromol. Chem. Rapid Commun.* **3**, 23 (1982).

28. R.W. Lenz, *Pure Appl. Chem.* **57**, 1537 (1985).

29. R.W. Lenz, *Faraday Disc. Chem. Soc.* **79**, 21 (1985).

30. K. Limura, N. Koide and R. Ohta, *Rep. Prog. Polym. Phys. Jpn.* **24**, 231 (1981).

31. A. Roviello, S. Santagata and A. Sirigu *Makrmol. Chem. Rapid Commun.* **4**, 281 (1983).

32. Q.-F. Zhou and R.W. Lenz, *J. Polym. Sci., Polym. Chem. Ed.* **21**, 3313 (1983).

33. G. R. Strobl and M. Schneider, *J. Polym. Sci. Polym. Phys. Edn.* **18**, 1343 (1980).

5. TABLES

Table 1

Experimental and Model Crystallographic Parameters of a Crystal Unit Cell of HMS-5

Miller Index* (h k l)	2θ (°)		d-spacing (Å)	
	data	model	data	model
(1 0 1)	16.4 (±0.2°)	16.6	5.4 (±0.1Å)	5.4
(1 1 0)	19.9 (±0.2°)	19.8	4.5 (±0.1Å)	4.5
(0 2 0)	22.2 (±0.6°)	22.8	4.0 (±0.1Å)	3.9
(0 0 2)	7.6 (±0.2°)	7.6	11.6 (±0.2Å)	11.7
(0 1 2)	14.3 (±0.6°)	13.7	6.2 (±0.3Å)	6.5
(1 2 1)	27.7 (±0.6°)	28.3	3.2(±0.1Å)	3.2
(0 2 2)	24.6 (±0.5°)	24.1	3.6 (±0.1Å)	3.7
(0 2 3)	25.7 (±0.3°)	25.5	3.5 (±0.1Å)	3.5

* Miller indices are assigned based on orthorhombic structure with lattice parameters given in Table 5

Table 2

Experimental and Model Crystallographic Parameters of a Crystal Unit Cell of HMS-6

Miller Index* (h k l)	2θ (°)		d-spacing (Å)	
	data	model	data	model
(1 1 0)	21.3 (±0.3°)	21.2	4.2 (±0.1Å)	4.2
(0 2 0)	19.3 (±0.2°)	19.3	4.6 (±0.1Å)	4.6
(0 1 2)	12.2 (±0.2°)	12.0	7.2 (±0.1Å)	7.3
(0 1 3)	14.9 (±0.4°)	14.5	5.9 (±0.2Å)	6.1
(1 3 1)	35.3 (±0.5°)	34.9	2.5 (±0.1Å)	2.6
(0 1 4)	16.7 (±0.6°)	17.4	5.3 (±0.2Å)	5.1
(1 1 4)	25.8 (±0.3°)	25.8	3.5 (±0.1Å)	3.5
(1 3 4)	38.7 (±0.6°)	38.0	2.3 (±0.1Å)	2.4

* Miller indices are assigned based on orthorhombic structure with lattice parameters given in Table 5

Table 3

Experimental and Model Crystallographic Parameters of a Crystal Unit Cell of HMS-7

Miller Index* (h k l)	2θ (°)		d-spacing (Å)	
	data (±0.6°)	model	data	model
(1 0 1)	12.2 (±0.2°)	12.1	7.3 (±0.1Å)	7.3
(1 1 0)	20.0 (±0.3°)	20.2	4.4 (±0.1Å)	4.4
(1 1 1)	16.5 (±0.2°)	16.5	5.4 (±0.1Å)	5.4
(0 2 0)	22.6 (±0.3°)	22.5	3.9 (±0.1Å)	4.0
(1 0 2)	9.5 (±0.2°)	9.5	9.3 (±0.1Å)	9.3
(1 1 2)	14.7 (±0.2°)	14.7	6.0 (±0.1Å)	6.0
(1 2 1)	24.9 (±0.6°)	25.6	3.6 (±0.1Å)	3.5
(0 2 2)	26.0 (±0.4°)	25.7	3.4 (±0.1Å)	3.5
(2 1 6)	24.0 (±0.3°)	23.9	3.7 (±0.1Å)	3.7

* Miller indices are assigned based on monoclinic structure with lattice parameters given in Table 5

Table 4

Experimental and Model Crystallographic Parameters of a Crystal Unit Cell of HMS-8

Miller Index* (h k l)	2θ (°)		d-spacing (Å)	
	data	model	data	model
(0 1 1)	11.4 (±0.2°)	11.5	7.8 (±0.2Å)	7.7
(1 0 1)	13.5 (±0.5°)	14.0	6.6 (±0.3Å)	6.3
(1 1 0)	21.9 (±0.4°)	21.5	4.1 (±0.1Å)	4.1
(0 2 0)	19.0 (±0.2°)	19.1	4.7 (±0.1Å)	4.7
(0 2 1)	20.6 (±0.4°)	20.2	4.3 (±0.1Å)	4.4
(1 3 0)	34.8 (±0.3°)	34.8	2.6 (±0.1Å)	2.6
(1 0 -1)	25.0 (±0.3°)	25.2	3.6 (±0.1Å)	3.5
(1 1 4)	16.6 (±0.2°)	16.6	5.3 (±0.1Å)	5.3

* Miller indices are assigned based on monoclinic structure with lattice parameters given in Table 5

Table 5

Thermal Transition Peak Temperatures for DMS Polycarbonates at 10°C/minute Scan Rate

Sample n	Crystallization Temp.(°C) T_c	Melting Temp.(°C) T_m
4	149	172
5	66	115
6	157	174
7	110	142
8	113	139
9	77	105
10	77	106
12	80	112

Table 6

Long period, Linear Crystallinity and Crystal Thickness for DMS-5-8 and HMS-5-8 Crystallized by Cooling at 5°C/min from the Melt to Room Temperature

Sample	L(Å) (±5Å)	χ_c (±0.01)	lc(Å) (±2Å)
DMS-5	230	0.20	32
DMS-6	189	0.28	45
DMS-7	218	0.29	67
DMS-8	191	0.28	47
HMS-5	214	0.26	44
HMS-6	215	0.21	33
HMS-7	234	0.25	46
HMS-8	230	0.18	29

Table 7

Long period, Linear Crystallinity and Crystal Thickness for Isothermally Crystallized Samples and Annealed Fibers

Sample	L(Å) (±5Å)	χ_c (±0.01)	lc(Å) (±2Å)
	Isothermally Crystallized at 124°C		
DMS-7	245	25	55
DMS-8	251	24	53
	Annealed Fiber		
HMS-7	196	24	39
DMS-7	173	27	40

6. Figures

Figure 1 WAXS intensity versus two theta for HMS-4-10, -12.

Figure 2 Interplanar spacing, d, versus flexible spacer number, n, for HMS polymers. a.) (□) higher value d-spacing and (●) lower value d-spacing for the two major interchain reflections shown in Figure 1; b.) (——) (020) and (- - - -) (110) interchain reflections grouped according to their Miller indices.

Figure 3 Flat film WAXS of hand drawn raw fibers: a.) HMS-5, b.) HMS-8. Fiber axis is vertical.

Figure 4 WAXS of hand drawn annealed fibers: a.) HMS-5 experimental pattern; b.) Sketch of HMS-5 pattern; c.) HMS-8 experimental pattern; d.) Sketch of HMS-8 pattern. Fiber axis is vertical. Spotty ring is from Si calibration standard.

Figure 5 WAXS intensity versus two theta for DMS-7.

Figure 6 DSC of DMS-4-10, 12 at 10°C/min: (a) cooling, and (b) heating.

Figure 7 DSC of DMS-7 and HMS-7 at 10°C/min: (a) cooling, and (b) heating.

Figure 8 DSC of (a) DMS-7 and (b) HMS-7 at various cooling rates.

Figure 9 Lorentz corrected SAXS intensity, Is^2 vs. s at room temperature for (a) DMS-7 and (b) HMS-7, cooled at -5°C/min from the melt.

Figure 10 Real-time Lorentz corrected SAXS intensity, Is^2 vs. s, Lowest curve marked 154°C represents the melt state. Crystallization at 124°C is recorded from t = 0 to t =340 seconds.

Fig. 1

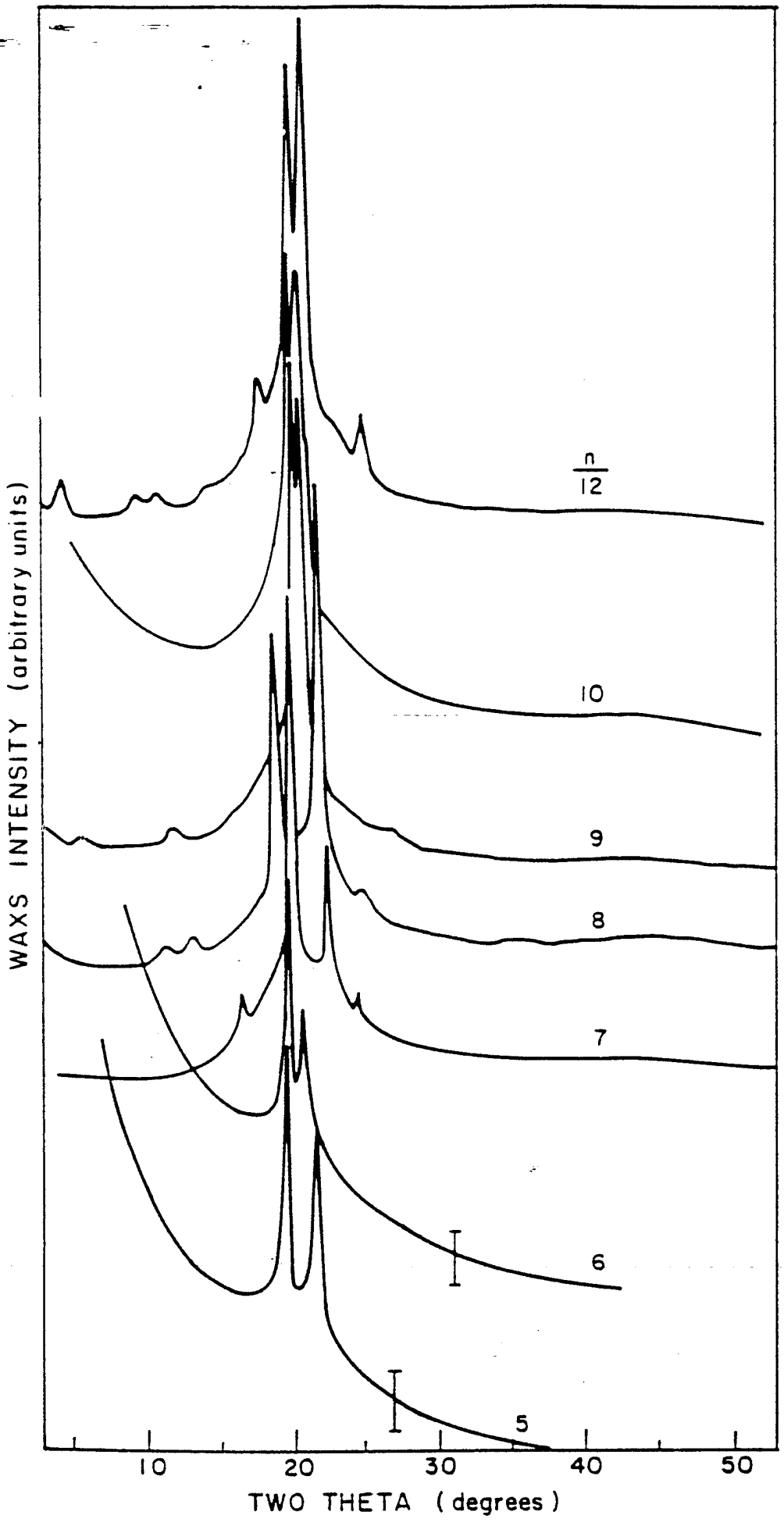
WAXS INTENSITY (arbitrary units)
n/12
10
9
8
7
6
5
10
20
30
40
50
TWO THETA (degrees)

Fig. 2a

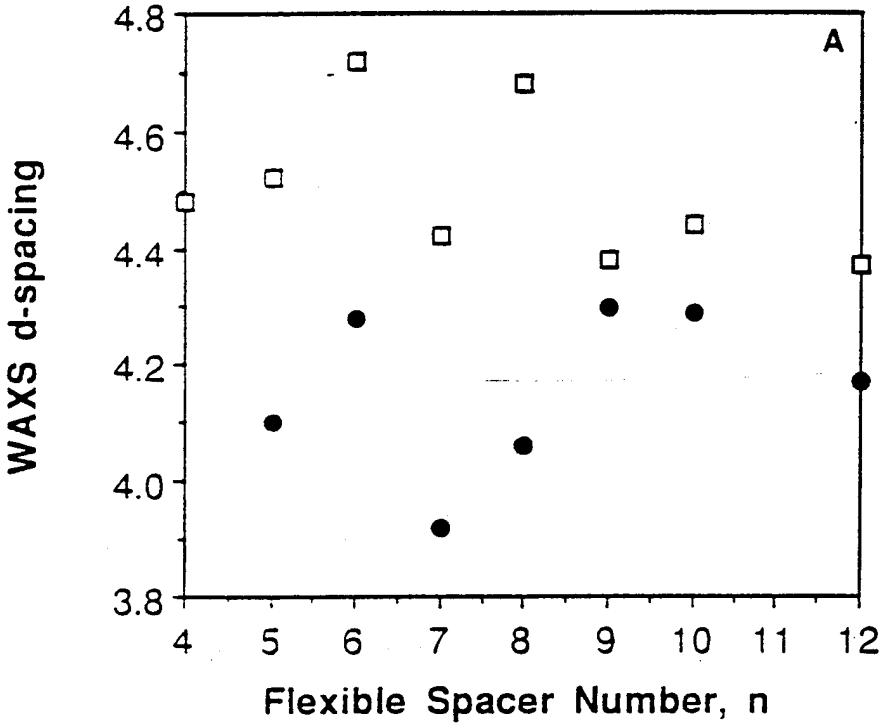
A
WAXS d-spacing
4.8
4.6
4.4
4.2
4.0
3.8
4
5
6
7
8
9
10
11
12
Flexible Spacer Number, n

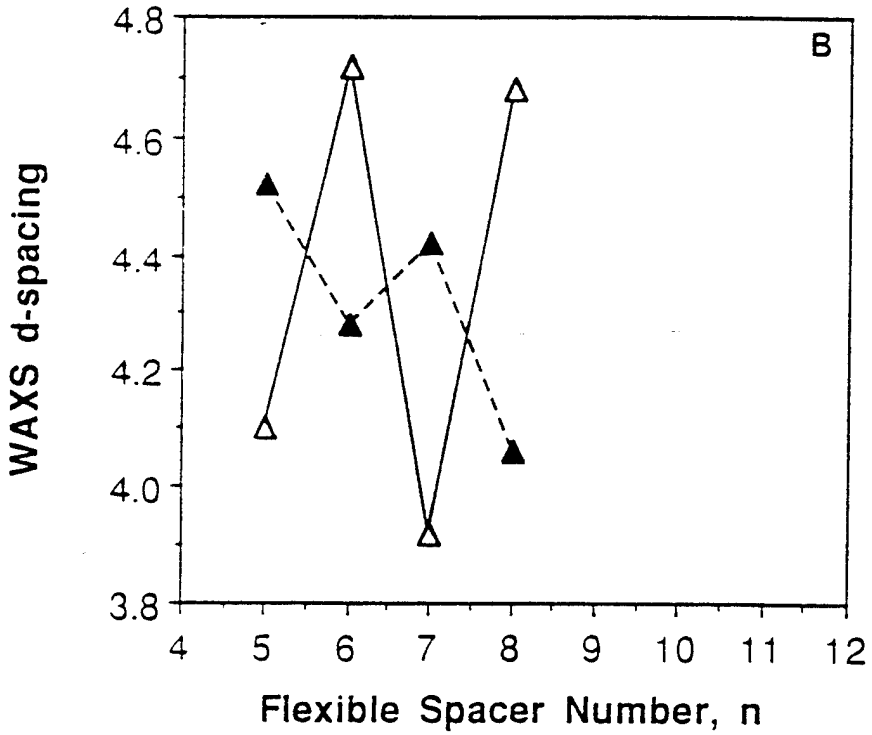
B
WAXS d-spacing
4.8
4.6
4.4
4.2
4.0
3.8
4
5
6
7
8
9
10
11
12
Flexible Spacer Number, n

Fig 3a

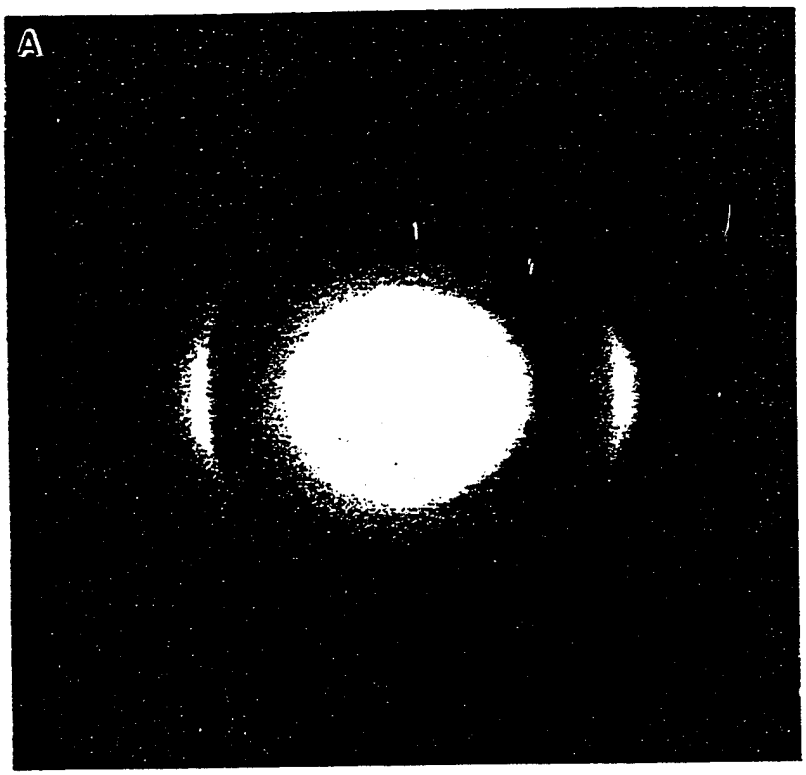


B

Fig. 4a

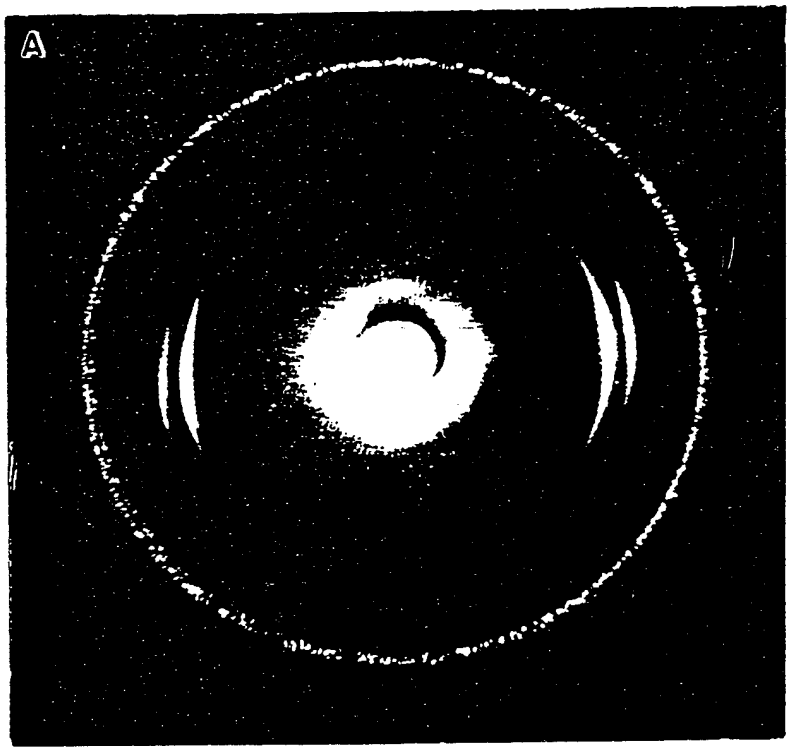

B

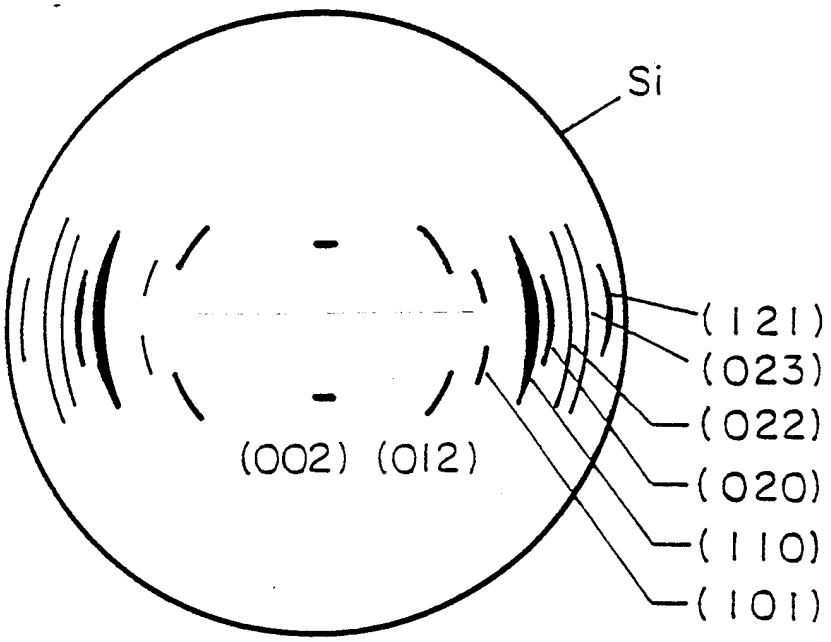


C

Fig. 4.1 2c

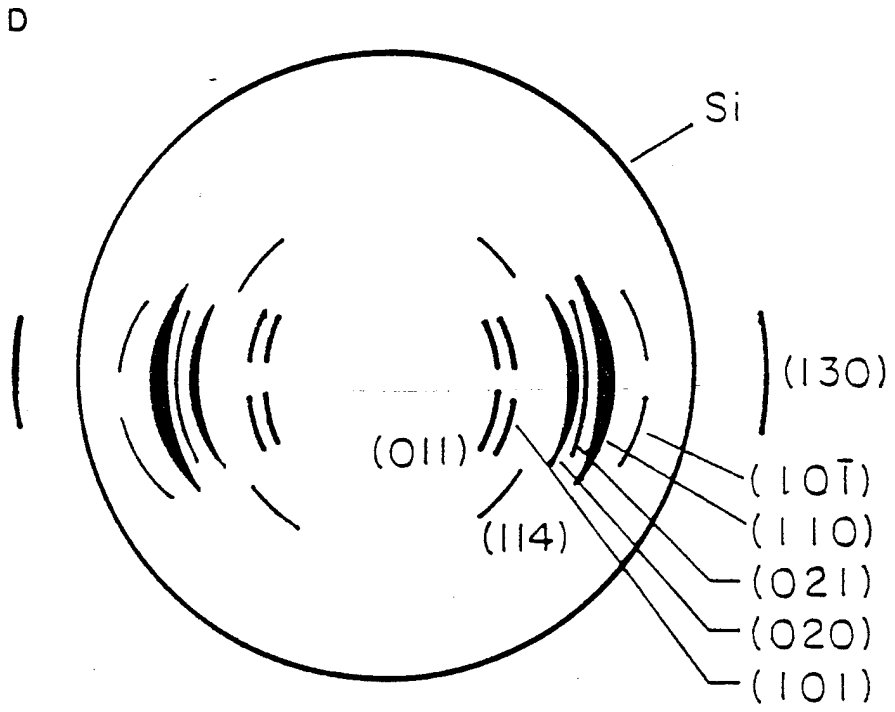

Fig. 5

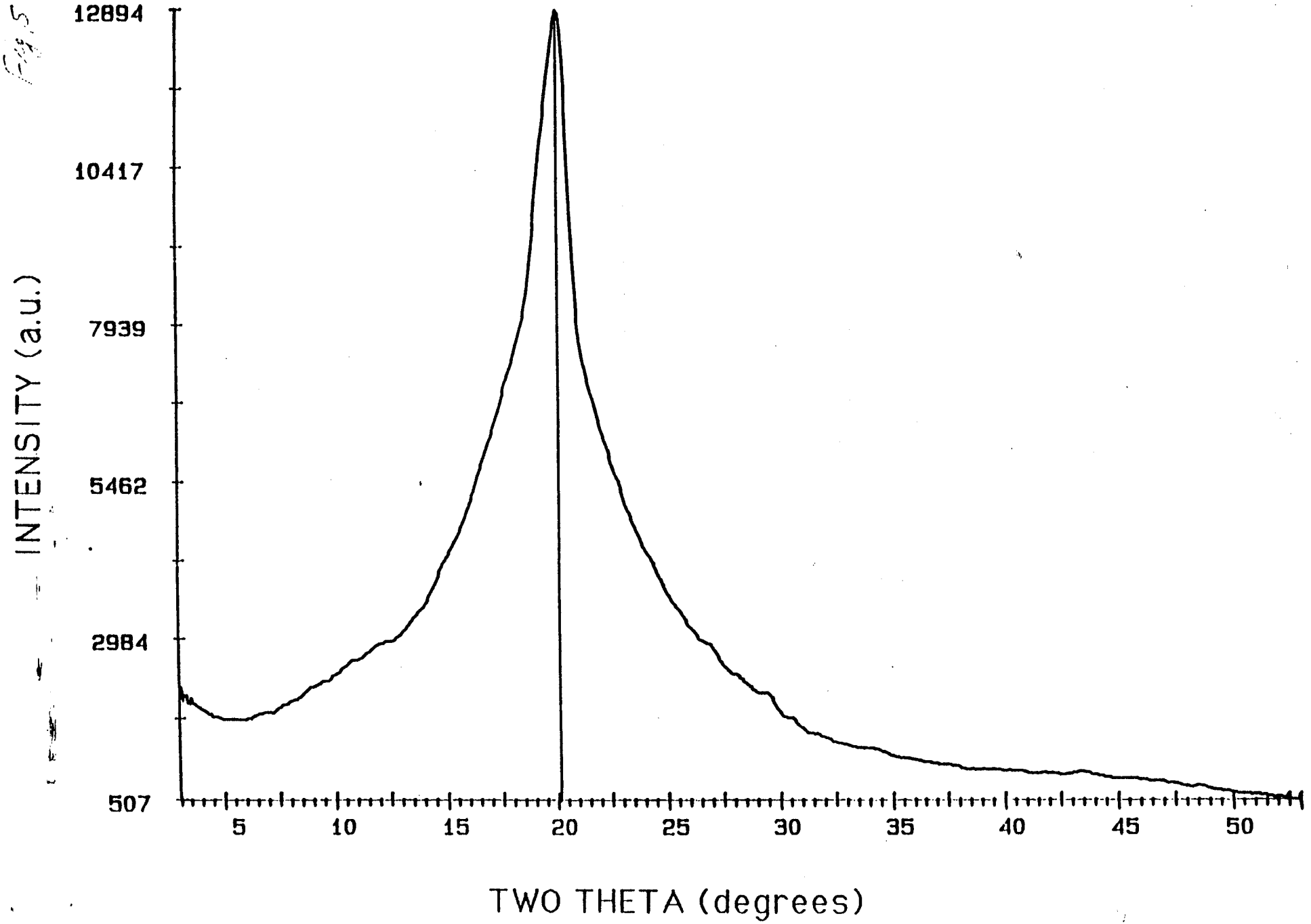
12894
10417
7939
5462
2984
507
INTENSITY (a.u.)
5
10
15
20
25
30
35
40
45
50
TWO THETA (degrees)

Fig. 6a

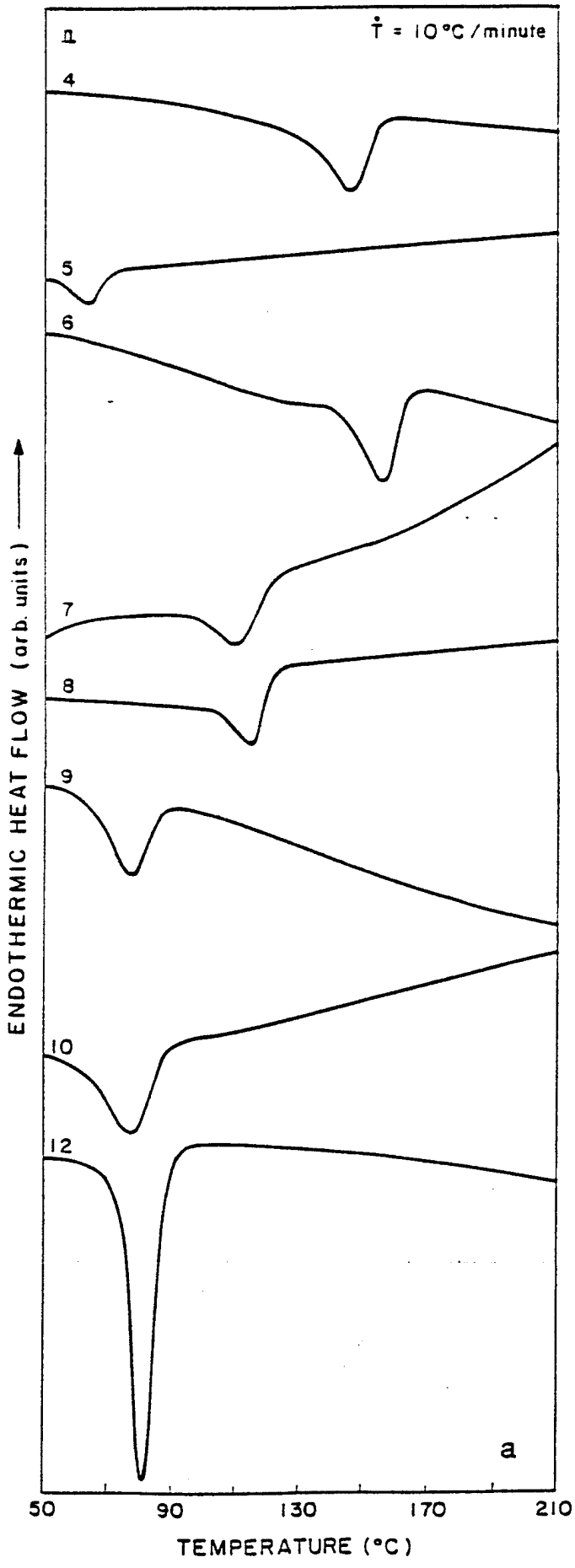
Ṫ = 10°C / minute
4
5
6
7
8
9
10
12
a
ENDOTHERMIC HEAT FLOW (arb. units)
50
90
130
170
210
TEMPERATURE (°C)

Fig 6b

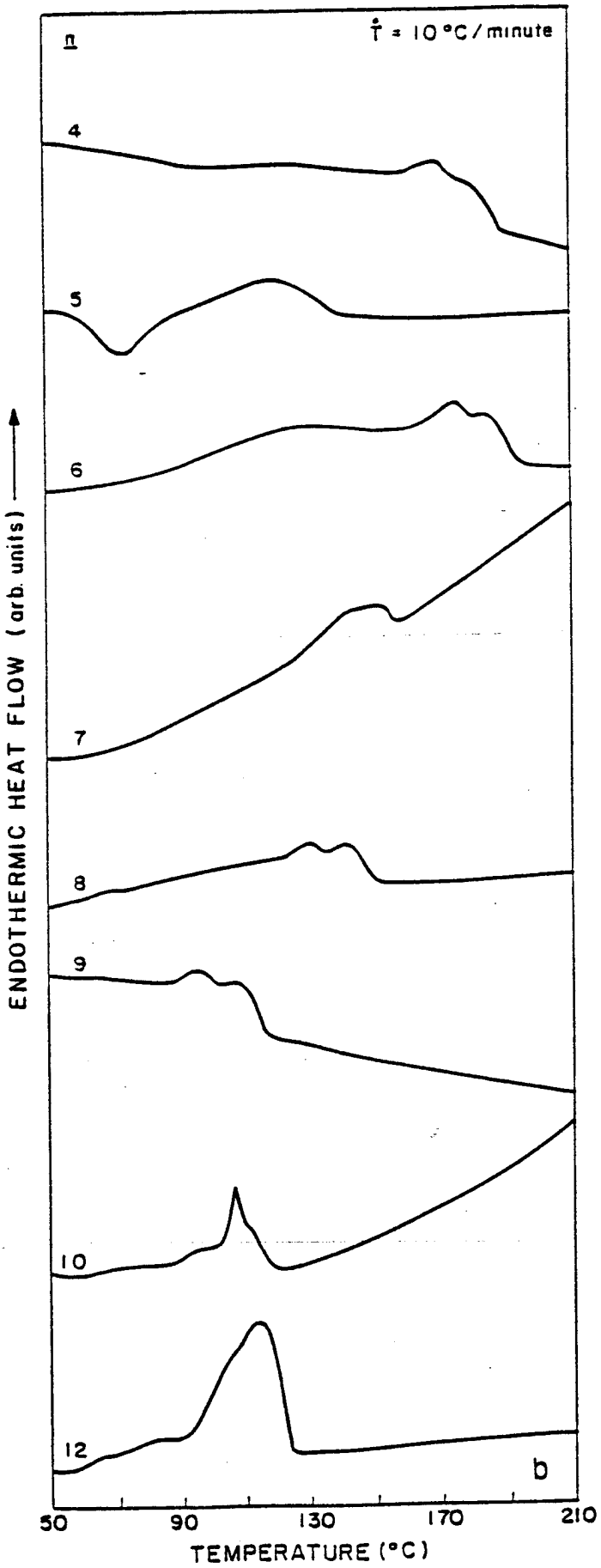
n
$\dot{T}$ = 10 °C / minute
4
5
6
7
8
9
10
12
b
ENDOTHERMIC HEAT FLOW (arb. units)
50
90
130
170
210
TEMPERATURE (°C)

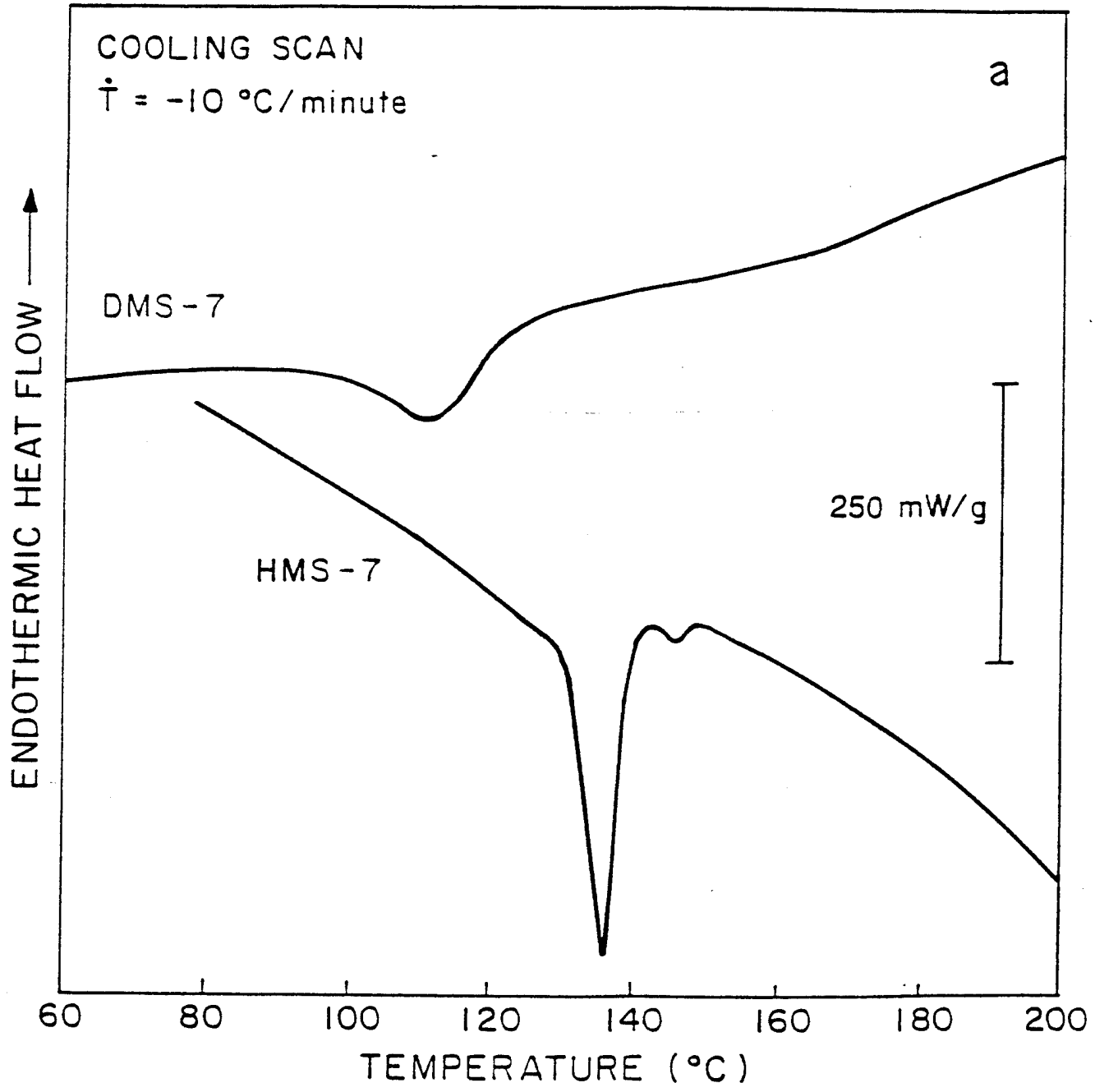
COOLING SCAN
Ṫ = -10 °C/minute
a
DMS-7
HMS-7
250 mW/g
ENDOTHERMIC HEAT FLOW
60
80
100
120
140
160
180
200
TEMPERATURE (°C)

Fig 4b

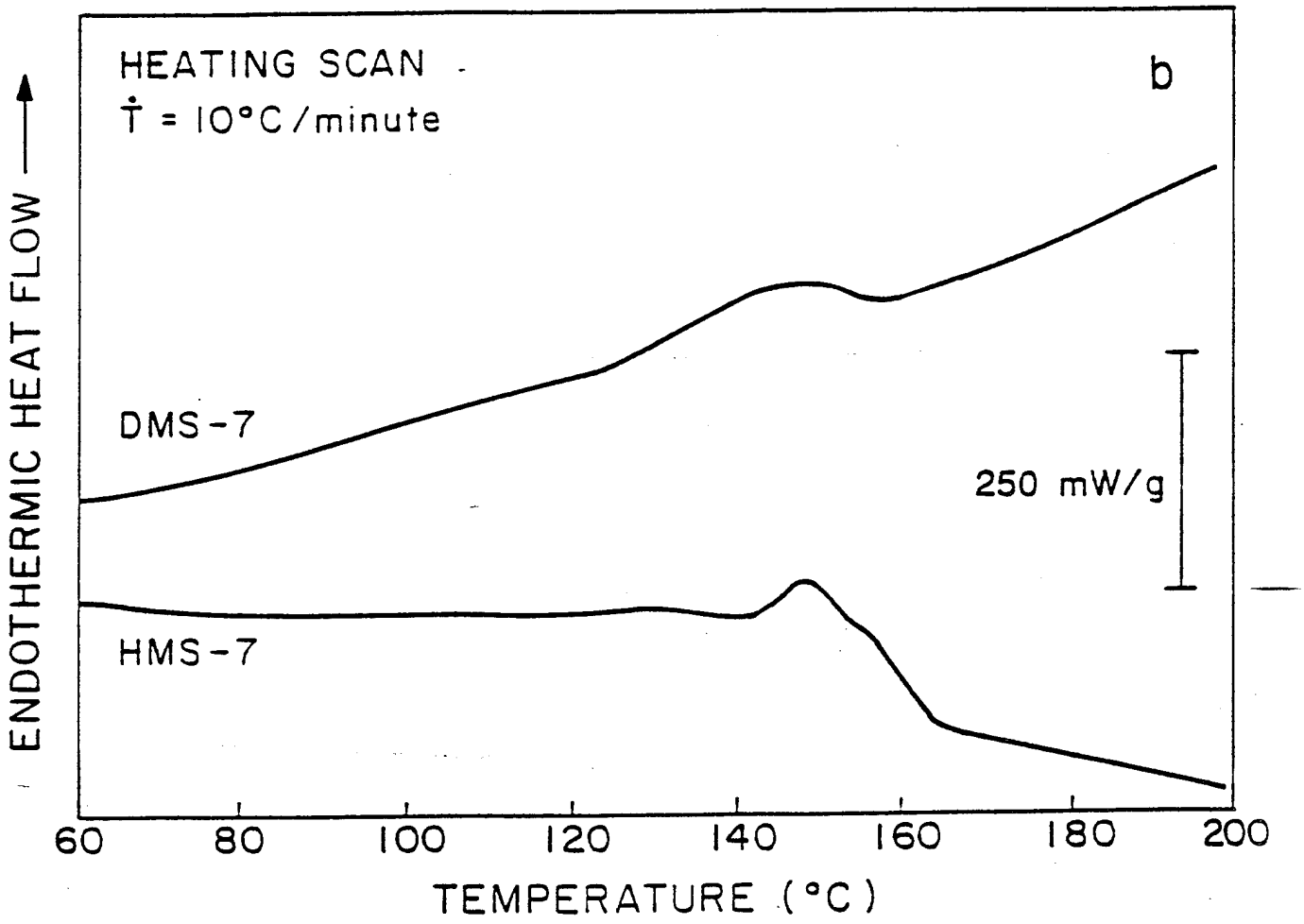
HEATING SCAN
$\dot{T}$ = 10°C/minute
b
DMS-7
HMS-7
250 mW/g
ENDOTHERMIC HEAT FLOW
60
80
100
120
140
160
180
200
TEMPERATURE (°C)

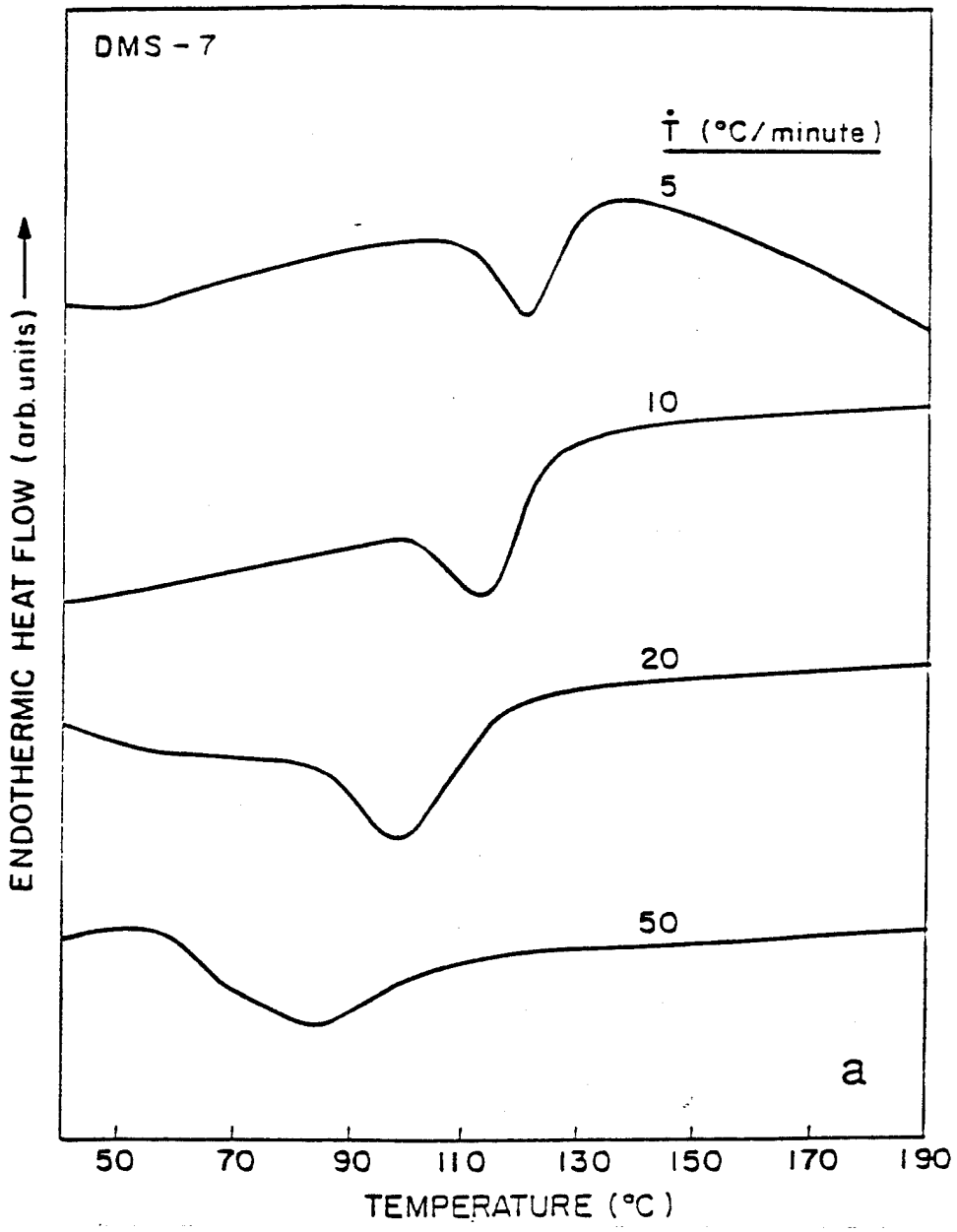
DMS - 7
Ṫ (°C/minute)
5
10
20
50
a
ENDOTHERMIC HEAT FLOW (arb. units)
50
70
90
110
130
150
170
190
TEMPERATURE (°C)

Fig 5b

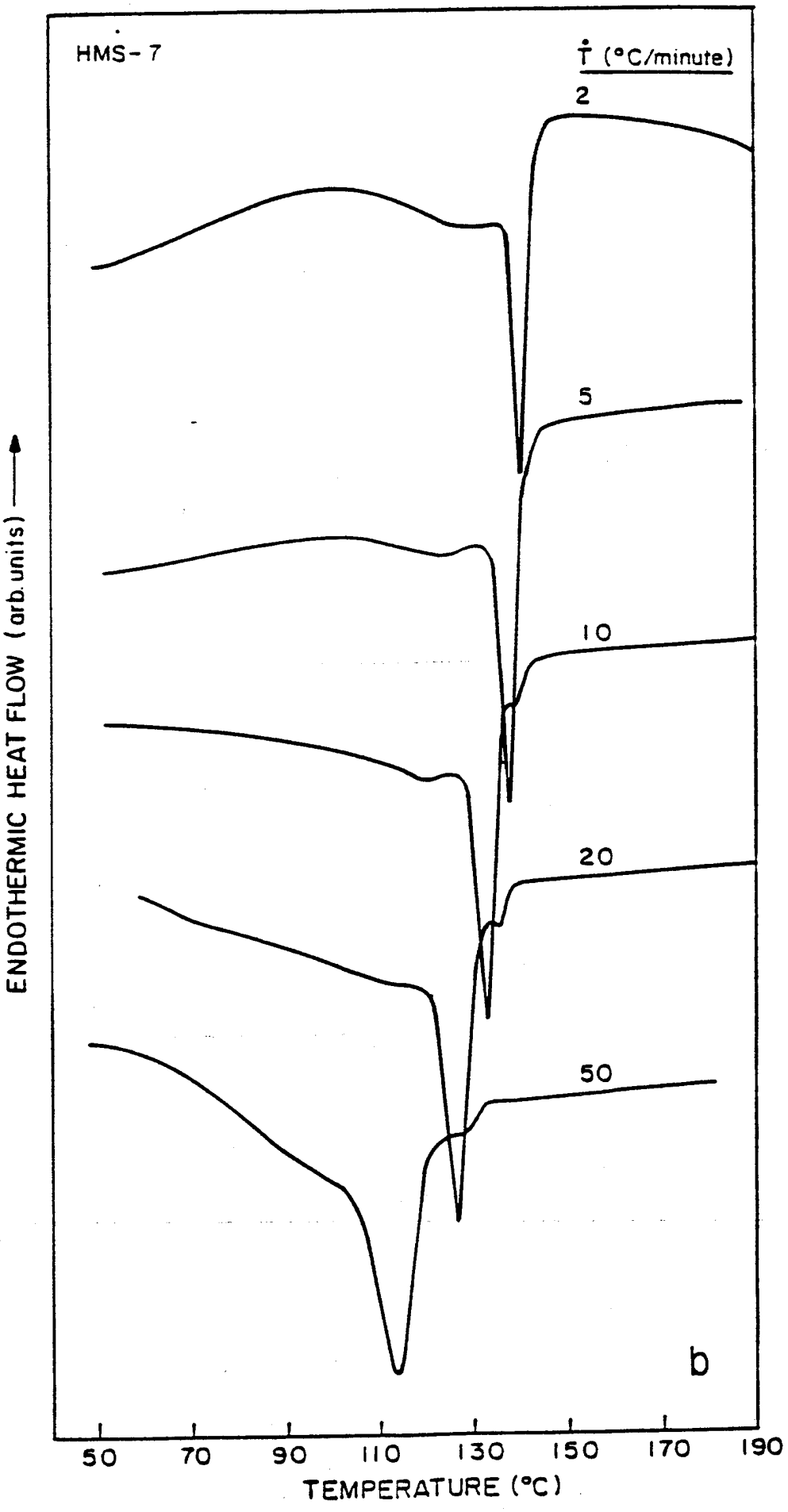
HMS-7
Ṫ (°C/minute)
2
5
10
20
50
b
ENDOTHERMIC HEAT FLOW (arb.units)
50
70
90
110
130
150
170
190
TEMPERATURE (°C)

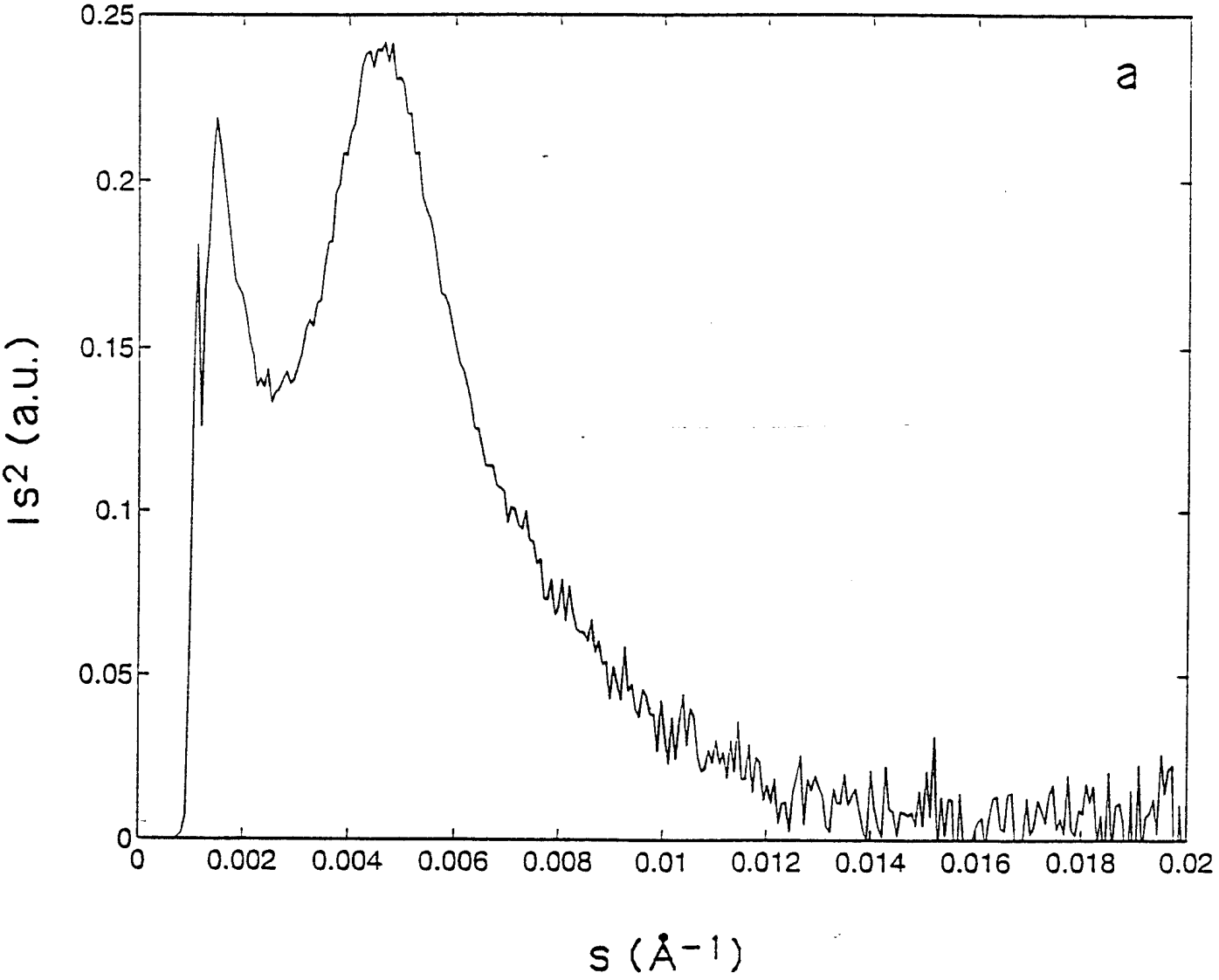
a
Is2 (a.u.)
s (Å-1)
0.25
0.2
0.15
0.1
0.05
0
0.002
0.004
0.006
0.008
0.01
0.012
0.014
0.016
0.018
0.02

Fig. 4b

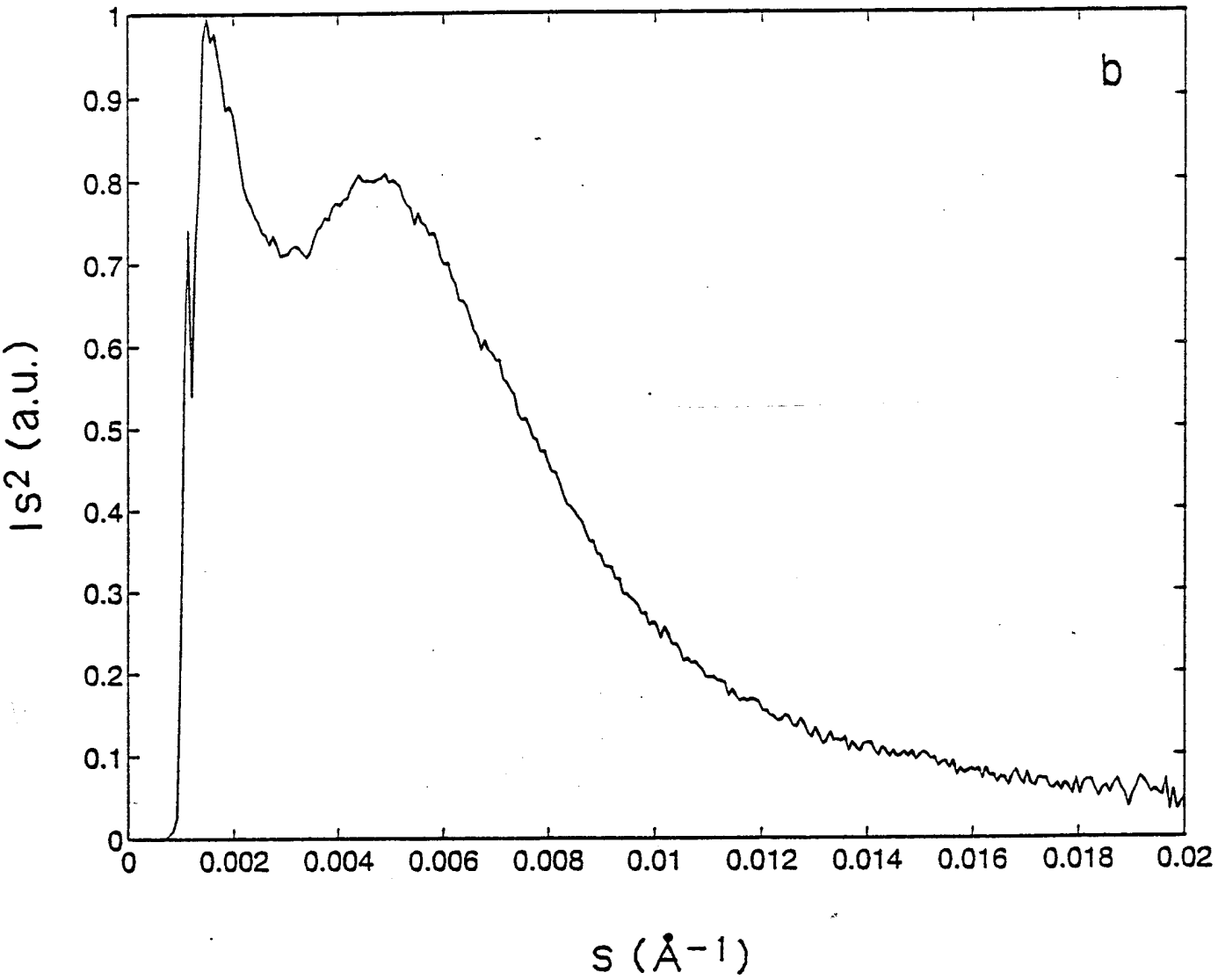
b
Is2 (a.u.)
s (Å-1)
0
0.1
0.2
0.3
0.4
0.5
0.6
0.7
0.8
0.9
1
0
0.002
0.004
0.006
0.008
0.01
0.012
0.014
0.016
0.018
0.02

Fig 10

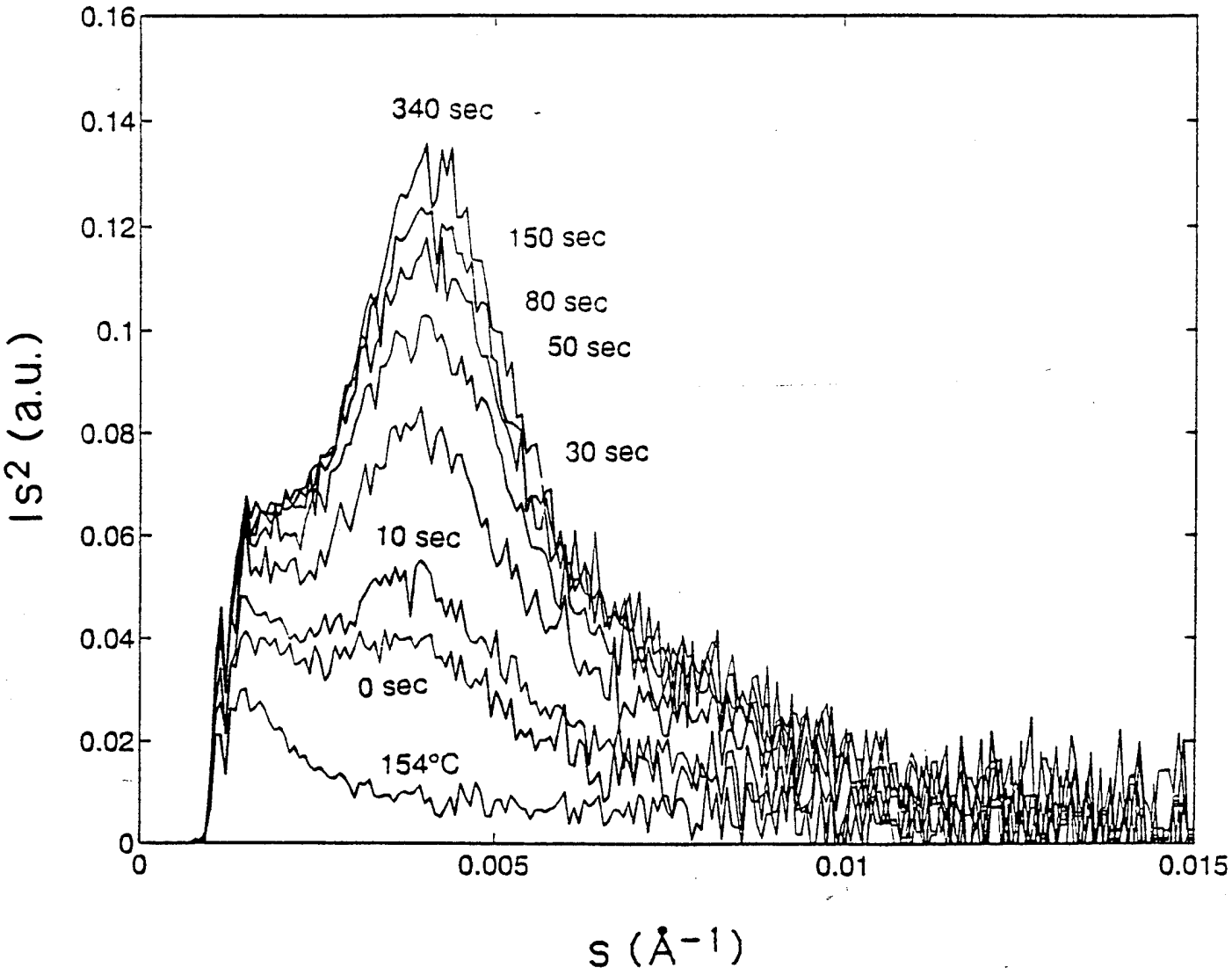
0.16
0.14
0.12
0.1
0.08
0.06
0.04
0.02
0
Is2 (a.u.)
340 sec
150 sec
80 sec
50 sec
30 sec
10 sec
0 sec
154°C
0
0.005
0.01
0.015
s (Å-1)